# Pharmacokinetic Analysis and Uptake of $^{18}$F-FBPA-Fr After Ultrasound-Induced Blood–Brain Barrier Disruption for Potential Enhancement of Boron Delivery for Neutron Capture Therapy

Feng-Yi Yang[1,2], Wen-Yuan Chang[1], Jia-Je Li[1], Hsin-Ell Wang[1], Jyh-Cheng Chen[1], and Chi-Wei Chang[3]

*[1]Department of Biomedical Imaging and Radiological Sciences, School of Biomedical Science and Engineering, National Yang-Ming University, Taipei, Taiwan; [2]Biophotonics and Molecular Imaging Research Center, National Yang-Ming University, Taipei, Taiwan; and [3]National PET/Cyclotron Center, Taipei Veterans General Hospital, Taipei, Taiwan*

Boronophenylalanine has been applied in clinical boron neutron capture therapy for the treatment of high-grade gliomas. The purpose of this study was to evaluate the pharmacokinetics of 4-borono-2-$^{18}$F-fluoro-L-phenylalanine-fructose ($^{18}$F-FBPA-Fr) in F98 glioma–bearing Fischer 344 rats by means of intravenous injection of $^{18}$F-FBPA-Fr both with and without blood–brain barrier disruption (BBB-D) induced by focused ultrasound (FUS). **Methods:** Dynamic PET imaging of $^{18}$F-FBPA-Fr was performed on the ninth day after tumor implantation. Blood samples were collected to obtain an arterial input function for tracer kinetic modeling. Ten animals were scanned for approximately 3 h to estimate the uptake of $^{18}$F radioactivity with respect to time for the pharmacokinetic analysis. Rate constants were calculated by use of a 3-compartment model. **Results:** The accumulation of $^{18}$F-FBPA-Fr in brain tumors and the tumor-to-contralateral brain ratio were significantly elevated after intravenous injection of $^{18}$F-FBPA-Fr with BBB-D. $^{18}$F-FBPA-Fr administration after sonication showed that the tumor-to-contralateral brain ratio for the sonicated tumors (3.5) was approximately 1.75-fold higher than that for the control tumors (2.0). Furthermore, the $K_1/k_2$ pharmacokinetic ratio after intravenous injection of $^{18}$F-FBPA-Fr with BBB-D was significantly higher than that after intravenous injection without BBB-D. **Conclusion:** This study demonstrated that radioactivity in tumors and the tumor-to-normal brain ratio after intravenous injection of $^{18}$F-FBPA-Fr with sonication were significantly higher than those in tumors without sonication. The $K_1/k_2$ ratio may be useful for indicating the degree of BBB-D induced by FUS. Further studies are needed to determine whether FUS may be useful for enhancing the delivery of boronophenylalanine in patients with high-grade gliomas.

**Key Words:** pharmacokinetics; focused ultrasound; blood–brain barrier; $^{18}$F-FBPA-Fr; boron neutron capture therapy

**J Nucl Med 2014; 55:616–621**
DOI: 10.2967/jnumed.113.125716

Boron neutron capture therapy (BNCT) is a binary cancer treatment system that requires the selective delivery of a boron-containing drug to the tumor and then irradiation with neutrons to yield high-linear-energy-transfer α particles and recoiling $^{7}$Li nuclei (*1–5*). Successful application of BNCT requires the selective delivery of $^{10}$B to the tumor, low levels in the surrounding tissue, and the delivery of sufficient thermal neutron fluence to the tumor site (*6,7*). Considerable efforts have been dedicated to the development of boron-delivering agents that could ensure a high tumor-to-normal tissue ratio of uptake of boron in tumors for BNCT (*8*). With the development of new techniques for the chemical synthesis of an effective agent, several new potential boron-delivering agents have emerged. However, drug delivery will have to be optimized because it is unlikely that any single agent will be capable of targeting most of the tumor cells.

Despite the fact that the blood–tumor barrier is more permeable than the blood–brain barrier (BBB), the efficacy of systemic chemotherapy in patients with brain tumors is poor because the selective permeability of the blood–tumor barrier still restricts the accumulation of drugs delivered to the tumors (*9*). Promising clinical results for the treatment of high-grade gliomas have been reported by several clinical groups in Japan (*10–13*), Sweden (*10,14*), and Finland (*15*). Barth et al. demonstrated that boron uptake in brain tumors and animal survival could be improved by BBB disruption (BBB-D) induced with a hyperosmotic solution of mannitol (*16,17*). It has been shown that the amount of boron in brain tumors and the tumor-to-normal brain ratio after BBB-D induced by mannitol injection are significantly higher than those for tumors without BBB-D (*18*). Although this approach induces BBB-D throughout the entire area of the brain supplied by the injected artery (*19,20*), the boron compound is rapidly cleared from the normal brain and persists at a higher level in the tumor.

Our previous studies showed that focused ultrasound (FUS) could noninvasively enhance the permeability of BBB in the local region (*21–23*). The degree of FUS-induced BBB-D is affected by several ultrasound parameters, including acoustic power, frequency, burst length, the duty cycle of the transducer, and the concentration and size of the ultrasound contrast agent (*24–26*). The use of therapeutic agents followed by sonication represents a feasible approach for enhanced local drug delivery and improved treatment efficacy

Received May 2, 2013; revision accepted Nov. 11, 2013.
For correspondence contact: Feng-Yi Yang, Department of Biomedical Imaging and Radiological Sciences, School of Biomedical Science and Engineering, National Yang-Ming University, Number 155, Section 2, Li-Nong St., Taipei 11221, Taiwan.
E-mail: fyyang@ym.edu.tw
Published online Feb. 13, 2014.

in brain tumors (*27,28*). Moreover, it has been demonstrated that boronophenylalanine (BPA) injection in combination with FUS exposure increases the accumulation of boron in brain tumors (*29*). An evaluation of micro-SPECT/CT imaging showed that FUS not only significantly increased the permeability of the BBB at the sonicated site but also significantly elevated the tumor-to-normal brain ratio for a drug in the focal region (*30,31*). Nuclear imaging may be useful for offering a good assessment of the extent of BBB-D and identifying the optimum therapeutic window for radiotherapy or chemotherapy of brain tumors with BBB-D induced by sonication.

In this study, we evaluated the pharmacokinetics of 4-borono-2-$^{18}$F-fluoro-L-phenylalanine-fructose ($^{18}$F-FBPA-Fr) after intravenous injection, both with and without BBB-D induced by FUS, in F98 glioma–bearing rats. The pharmacokinetics of $^{18}$F-FBPA-Fr after sonication were monitored with noninvasive PET to demonstrate the optimal treatment protocol for thermal neutron irradiation. Furthermore, the rate constants $K_1$, $k_2$, $k_3$, and $k_4$ were derived from dynamic small-animal PET images (Fig. 1).

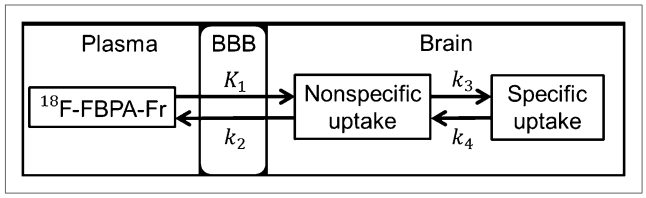


**FIGURE 1.** Pharmacokinetics of $^{18}$F-FBPA-Fr analyzed by 3-compartment model for $K_1$ (mL/g/min), $k_2$ ($min^{-1}$), $k_3$ ($min^{-1}$), and $k_4$ ($min^{-1}$). $K_1$ and $k_2$ represent forward transport and reverse transport of $^{18}$F-FBPA-Fr across BBB, respectively. $k_3$ and $k_4$ are anabolic and reverse-process rate constants, respectively.

## MATERIALS AND METHODS

### Glioma Tumor Model and $^{18}$F-FBPA-Fr Preparation

Male Fischer 344 rats (11–13 wk; approximately 250–280 g) were anesthetized with an intraperitoneal administration of pentobarbital at a dose of 40 mg/kg of body weight. Next, $10^5$ F98 rat glioma cells in 10 μL of Hanks balanced salt solution without $Mg^{2+}$ and $Ca^{2+}$ were injected into the brain. The glioma cells were stereotactically injected into a single location in the right hemisphere (5.0 mm posterior and 3.0 mm lateral to the bregma) of each rat at a depth of 5.0 mm from the brain surface. Next, the holes in the skull were sealed with bone wax, and the wound was flushed with iodinated alcohol. All procedures were performed according to the guidelines of and were approved by the Animal Care and Use Committee of the National Yang-Ming University. $^{18}$F-FBPA-Fr was prepared by the method described in a previous report (*32*). The radiochemical purity of $^{18}$F-FBPA-Fr was greater than 97%.

### Focused Ultrasound System and Exposure

Pulsed FUS exposures were generated with a 1.0-MHz, single-element focused transducer (A392S; Panametrics). The entire FUS system setup was described in our previous study (*33*). The half maximum of the pressure amplitude of the focal zone had a diameter and a length of 3 mm and 26 mm, respectively. The ultrasound contrast agent (SonoVue; Bracco International) was injected into the tail vein of the rats approximately 15 s before sonication. The sonication was precisely targeted with a stereotactic apparatus (Stoelting) that used the bregma of the skull as an anatomic landmark. Sonication was applied to the tumor region of 5 glioma-bearing rats on day 9 after tumor cell implantation. The focal zone of the ultrasound beam was delivered to a location in the right brain hemisphere centered at the tumor injection site. The sonication parameters were as follows: an acoustic power of 2.86 W (corresponding to a peak negative pressure of 0.7 MPa) with an ultrasound contrast agent injection of 300 μL/kg, a pulse repetition frequency of 1 Hz, a duty cycle of 5%, and a sonication time of 60 s.

### Dynamic PET Imaging

Dynamic small-animal PET images of the F98 glioma–bearing rats were obtained with a FLEX Triumph preclinical imaging system (Gamma Medica-Ideas, Inc.). The sensitivity and spatial resolution of the FLEX Triumph PET/SPECT/CT scanner were 1.1% and 0.91 mm, respectively. Animals were anesthetized by inhalation of 2% isoflurane in oxygen at 2 L/min in the prone position. Small-animal PET/CT was performed on day 9 after tumor cell implantation. For evaluation of the effect of BBB-D induced by FUS, each rat received a bolus injection into the tail vein of $^{18}$F-FBPA-Fr at a dose of 22.2 MBq for both brain tumors with BBB-D and brain tumors without BBB-D. Dynamic data acquisition was obtained with several frames at short intervals, followed by five 30-min frames up to 3 h after injection. The images were viewed and quantified with AMIDE (A Medical Imaging Data Examiner) software (free software provided by SourceForge) (*34*). Spheric regions of interest (radius, 2.5 mm) under the skull defect were manually pinpointed at the sonicated site and in the same region of the contralateral brain. The mean radioactivity within the region subjected to BBB-D at various time intervals was determined and compared with the results obtained for the equivalent region of the contralateral brain. Time–activity curves were plotted for both the tumor and the contralateral (normal) brain.

### Pharmacokinetic Analysis

Arterial blood samples were obtained during dynamic small-animal PET scanning; a total of 14 samples (0.1 mL each) were collected over a period of 3 h. The blood was spun in a microcentrifuge, and red cells and plasma were separated for inherent circulation plasma substrate measurements for each animal. The radioactivity of plasma samples was assayed with a γ scintillation counter and was expressed in kBq/mL of plasma sample. The pharmacokinetic parameters of the tissue could be estimated from the dynamically acquired small-animal PET images. with the data for plasma sample radioactivity as the arterial input function. The pharmacokinetics of $^{18}$F-FBPA-Fr were analyzed by use of a modified 3-compartment model for $K_1$ (mL/g/min), $k_2$ ($min^{-1}$), $k_3$ ($min^{-1}$), and $k_4$ ($min^{-1}$) (Fig. 1) (*35*). The rate constants ($K_1$, $k_2$, $k_3$,

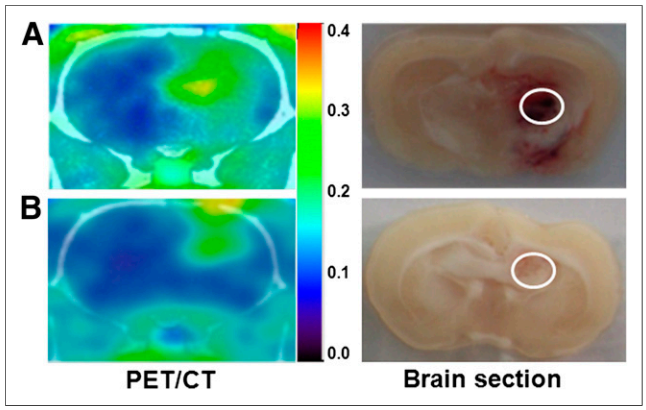


**FIGURE 2.** Small-animal PET/CT images of F98 glioma–bearing Fischer 344 rats and corresponding brain sections of tumors both with (A) and without (B) sonication by FUS. Regions targeted by FUS are circled in tumors in right hemisphere.

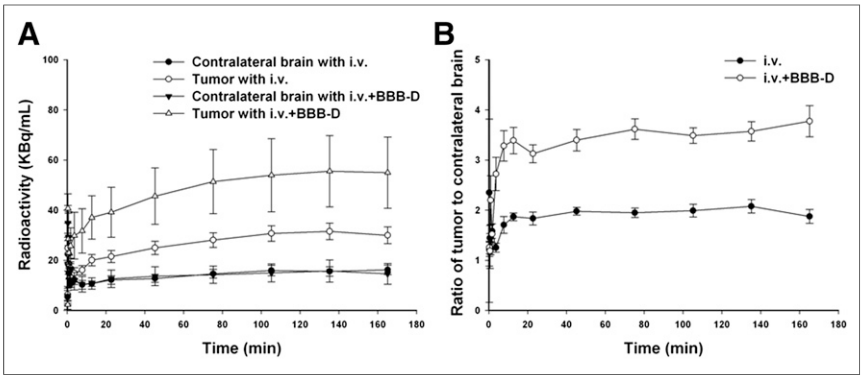


**FIGURE 3.** Pharmacokinetics of $^{18}$F-FBPA-Fr in glioma-bearing rats, calculated from small-animal PET. (A) Time–activity curves for $^{18}$F-FBPA-Fr in tumors and contralateral brains of glioma-bearing rats. Data were obtained from dynamic small-animal PET images after intravenous (i.v.) injection of $^{18}$F-FBPA-Fr both with and without BBB-D. (B) Tumor-to-contralateral brain ratio for $^{18}$F-FBPA-Fr, derived from data in A. Each point represents mean ± SEM for 5 rats.

and $k_4$) were calculated by nonlinear regression with PMOD software (version 3.0; PMOD Technologies).

### Histology

Two glioma-bearing rats from the FUS exposure group and 2 tumor-bearing control rats (no FUS exposure) were sacrificed after dynamic PET scanning for histologic examination. The rats were perfused with saline and 10% neutral buffered formalin. The brains were removed, embedded in paraffin, and then serially sectioned into 6-μm-thick slices. The slices were stained with hematoxylin and eosin to visualize the general cellular structure. Staining by terminal deoxynucleotidyl transferase–mediated dUTP nick-end labeling (TUNEL) (DeadEnd Colorimetric TUNEL system; G7130; Promega) was performed to detect DNA fragmentation and apoptotic bodies within the cells. Photomicrographs of brain sections stained with hematoxylin and eosin and by TUNEL were obtained by use of a Mirax Scan digital microscope slide scanner (3D Histech) with a Plan-Apochromat 20×/0.8 objective (Carl Zeiss). The serial histology images were annotated with Pannoramic Viewer software (3D Histech).

### Statistical Analysis

All data are shown as mean ± SEM. Statistical analysis was performed with an unpaired Student $t$ test. The level of statistical significance was set at a $P$ value of less than or equal to 0.05.

## RESULTS

In the small-animal PET/CT images of glioma-bearing rats, high contrast was seen in brain tumors both with and without sonication but especially in the sonicated tumors (Fig. 2). Moreover, the corresponding brain sections were observed for tumor identification after small-animal PET/CT scanning (Fig. 2). Hemorrhage in the tumor region was due to BBB-D after FUS exposure. The time–activity curves derived from dynamic small-animal PET/CT images for $^{18}$F-FBPA-Fr in the tumor and the contralateral (normal) brain are shown in Figure 3A. No significant differences in $^{18}$F-FBPA-Fr uptake were found in the tumor and the contralateral brain despite the BBB-D for the tumor. Compared with the contralateral brain, the tumor showed a significant accumulation of radioactivity. Furthermore, the uptake of $^{18}$F-FBPA-Fr in the tumor was significantly increased by BBB-D after FUS. Both of the derived tumor-to-contralateral brain ratios reached a plateau at 15 min after $^{18}$F-FBPA-Fr administration (Fig. 3B). The mean tumor-to-contralateral brain ratios from 15 min to 165 min after intravenous injection of $^{18}$F-FBPA-Fr both with and without BBB-D were approximately 3.5 and 2.0, respectively.

No significant differences in the time–activity curves for $^{18}$F-FBPA-Fr in plasma after intravenous injection were found both with and without BBB-D. These data were used as the arterial input function for calculating the pharmacokinetic parameters by use of tracer kinetic modeling (Fig. 4). Each point on the curve represented plasma sampling at a specific point during the time frame. The rate constants $K_1$, $k_2$, $k_3$, and $k_4$ derived from the arterial input function for the intravenous injection of $^{18}$F-FBPA-Fr with BBB-D are shown in Table 1.

Next, the $K_1/k_2$ ratio was obtained from a pharmacokinetic analysis of blood from the same rat as that used for the data shown in Table 1. Regression analysis (Fig. 5A) revealed a linear relationship between the radioactivity in the tumor and $K_1/k_2$, quantified as tumor radioactivity (KBq/mL) = $0.0376 \times K_1/k_2 - 0.172$ ($R^2 = 0.851$). Figure 5B shows the linear regression of $K_1/k_2$ with the tumor-to-contralateral brain ratio, quantified as tumor-to-contralateral brain ratio = $0.6574 \times K_1/k_2 - 0.6642$ ($R^2 = 0.906$).

Figure 6 shows mild scattered extravasation of red blood cells and TUNEL-positive apoptotic cells in the tumor tissues treated with $^{18}$F-FBPA-Fr and sonication relative to the tumor tissues treated with $^{18}$F-FBPA-Fr alone.

## DISCUSSION

The success of BNCT will depend mainly on the differential uptake of boron in tumors and normal tissues. When BPA is complexed with fructose, its accumulation in tumors has been proven to increase because of enhanced solubility (*36*). Previous studies

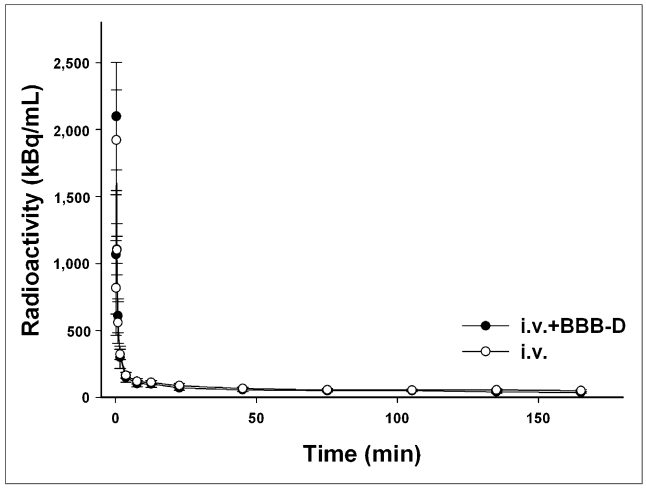


**FIGURE 4.** Time–activity curves for $^{18}$F-FBPA-Fr in plasma of F98 glioma–bearing rats after intravenous (i.v.) injection of $^{18}$F-FBPA-Fr both with and without BBB-D. Each point represents mean ± SEM for 5 rats.

**TABLE 1**
Rate Constants for Brain Tumors After Intravenous Injection of $^{18}$F-FBPA-Fr Both With and Without FUS-Induced BBB-D

| Rate constant or ratio | Intravenous injection of $^{18}$F-FBPA-F | Intravenous injection of $^{18}$F-FBPA-F + BBB-D |
|---|---|---|
| $K_1$ (mL/g/min) | 0.009 ± 0.004 | 0.011 ± 0.001 |
| $k_2$ (min$^{-1}$) | 0.031 ± 0.013 | 0.006 ± 0.0006 |
| $k_3$ (min$^{-1}$) | 0.54 ± 0.51 | 0.0004 ± 0.0003 |
| $k_4$ (min$^{-1}$) | 0.32 ± 0.24 | 2.3 ± 1.5 |
| $K_1/k_2$ | 0.41 ± 0.11 | 1.79 ± 0.23* |

*$P$ value for comparison of group receiving BBB-D with group not receiving BBB-D was 0.006.
Each value represents mean ± SEM for 5 rats.

reported that the pharmacokinetics of $^{18}$F-FBPA-Fr were similar to those of BPA (*18,37*). $^{18}$F-FBPA-Fr showed specific tumor uptake in F98 glioma–bearing rats and could be used as a probe for BPA complexed with fructose in clinical BNCT. In the present study, we used noninvasive small-animal PET/CT imaging to investigate the pharmacokinetics of $^{18}$F-FBPA-Fr after intravenous administration both with and without BBB-D induced by FUS.

To allow more $^{18}$F-FBPA-Fr to diffuse into the brain, hyperosmotic BBB-D was applied in preclinical BNCT. Compared with BNCT alone, BNCT with BBB-D showed significantly increased treatment efficacy and animal survival (*38,39*). Detailed pharmacokinetics after intravenous and intracarotid injections of $^{18}$F-FBPA-Fr and BPA, both with and without osmotic BBB-D, were reported in our previous study (*18*). The amount of boron in the tumor and the tumor-to-normal brain ratio after intracarotid injection of BPA with osmotic BBB-D were significantly higher than those produced by other delivery routes without BBB-D. For BNCT to be successful, it is essential not only to maximize tumor boron uptake but also to minimize boron concentrations in normal brain tissue. Neurotoxicity attributable to BBB-D combined with BPA or sodium sulfhydryl borane never was observed. However, BBB-D more effectively targeted infiltrating tumor cells (*40*). Therefore, targeted BBB-D induced by FUS could provide a powerful approach for local enhancement of boron uptake in the tumor region with minimal damage in the surrounding normal brain tissue.

The quantitative PET data indicated that the tumor-to-contralateral brain ratio in a glioma-bearing rat was 1.75-fold higher after intravenous injection of $^{18}$F-FBPA-Fr with BBB-D than after intravenous injection without BBB-D (Fig. 3B). Intravenous injection of BPA with FUS-induced BBB-D may be a better delivery method because this route is safer than intracarotid injection with hyperosmotic BBB-D used in previous studies. However, the bioeffects of ultrasound on brain tissue are still unknown, and further investigations of FUS are needed.

The modified 3-compartment model shown in Figure 1 indicated that an increase in BBB permeability was promoted by $K_1$ and suppressed by $k_2$. After the intravenous injection of $^{18}$F-FBPA-Fr with BBB-D, a mild increase in $K_1$ and a significant decrease in $k_2$ were seen (Table 1). These data indicated that $^{18}$F-FBPA-Fr was transported from the brain into the blood more readily after FUS-induced BBB-D. The $K_1/k_2$ ratio was significantly higher (~4.37-fold) after intravenous injection of $^{18}$F-FBPA-Fr with BBB-D than after intravenous injection without BBB-D. As described earlier, a decrease in $k_2$ was the principal factor affecting the $K_1/k_2$ ratio of $^{18}$F-FBPA-Fr after FUS-induced BBB-D. High interstitial fluid pressure is known to reduce the driving force for extravasation in tumors despite large gaps in the endothelium and greatly confining the transport of drugs (*41*). The effect of FUS on the $K_1/k_2$ ratio was consistent with the hypothesis that the enhanced extravasation of $^{18}$F-FBPA-Fr resulted partly from the decrease in high interstitial fluid pressure after FUS exposure.

An important requirement for BNCT is the accumulation of boron compounds in the tumor. The tumor-to-normal tissue ratio is another key requirement for determining the optimal neutron irradiation time for BNCT to minimize irradiation of normal tissues. Analysis of the $K_1/k_2$ ratio with boron tumor uptake or the tumor-to-contralateral brain ratio after FUS-induced BBB-D revealed that the values exhibited a good correlation (Fig. 5). Furthermore, the results revealed that the intravenous injection of $^{18}$F-FBPA-Fr with BBB-D would result in a higher level of tumor uptake of BPA and a higher tumor-to-contralateral brain ratio. Thus, the $K_1/k_2$ ratio may offer an indication of the extent of FUS-induced BBB-D and provide excellent feedback information to the operator. In ongoing studies, we plan to attempt to enhance the efficacy of BNCT by FUS exposure in animal brain tumor models.

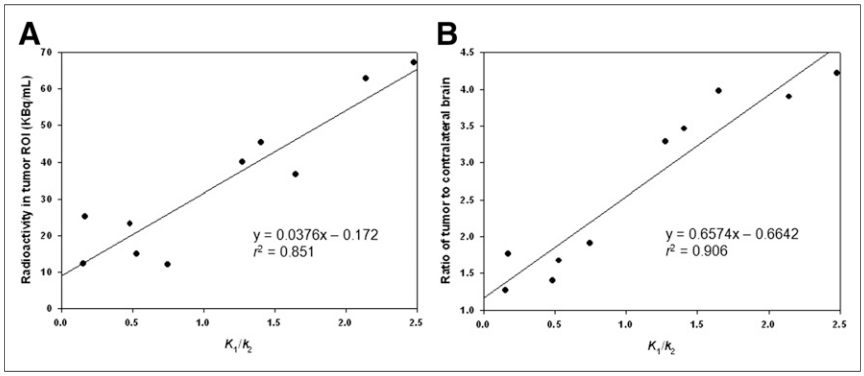


**FIGURE 5.** Correlations of $K_1/k_2$ ratio with radioactivity in tumor region of interest (ROI) and tumor-to-contralateral brain ratio. (A) Correlation between $K_1/k_2$ ratio and radioactivity in tumor ROI. (B) Correlation between $K_1/k_2$ ratio and tumor-to-contralateral brain ratio. Each point represents 1 rat. Mean radioactivity in tumor ROI and tumor-to-contralateral brain ratio were derived from small-animal PET images after intravenous injection of $^{18}$F-FBPA-Fr both with and without BBB-D.

## CONCLUSION

Investigation of the pharmacokinetics of $^{18}$F-FBPA-Fr with small-animal PET/CT

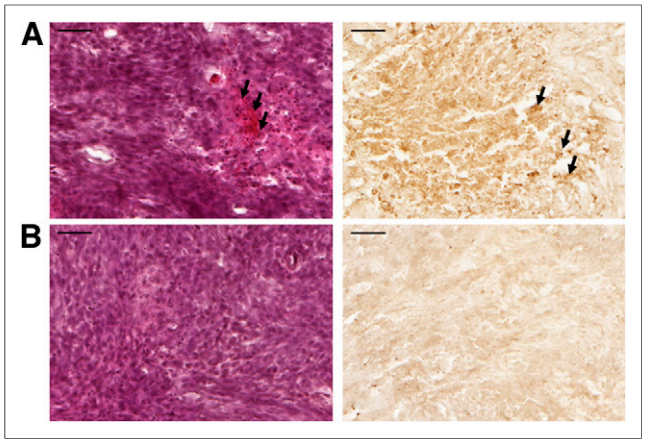


**FIGURE 6.** Histologic observations. Nine days after tumor implantation, glioma-bearing rats given $^{18}$F-FBPA-Fr both with (A) and without (B) sonication were sacrificed for staining with hematoxylin and eosin (left) and by TUNEL (right) (scale bar, 50 μm). Arrows indicate hemorrhages and apoptotic cells.

imaging revealed that FUS not only significantly increased the accumulation of boron in the sonicated tumor but also significantly elevated the tumor-to-normal brain ratio in the focal region. The $K_1/k_2$ ratio could be used to evaluate boron uptake in the tumor and the tumor-to-normal brain ratio and could provide an indication of the extent of FUS-induced BBB-D. This noninvasive nuclear imaging method may be a promising quantitative approach for optimizing the therapeutic window in future applications of BNCT.

## DISCLOSURE

The costs of publication of this article were defrayed in part by the payment of page charges. Therefore, and solely to indicate this fact, this article is hereby marked "advertisement" in accordance with 18 USC section 1734. This study was supported by grants from the National Science Council of Taiwan (NSC 101-2320-B-010-036-MY3, NSC 102-2221-E-010-005-MY3, NSC 100-2321-B-010-010, and NSC 99-2321-B-010-017), the Cheng Hsin General Hospital Foundation (102F218C11 and 101F195CY18), the Taipei Veterans General Hospital (VGH99A-026 and VGH100A-045), the Biophotonics and Molecular Imaging Research Center, and the Ministry of Education Aim for the Top University Plan. No other potential conflict of interest relevant to this article was reported.

## REFERENCES

1. Sweet WH. Early history of development of boron neutron capture therapy of tumors. *J Neurooncol.* 1997;33:19–26.
2. Asbury AK, Ojemann RG, Nielsen SL, Sweet WH. Neuropathologic study of fourteen cases of malignant brain tumor treated by boron-10 slow neutron capture radiation. *J Neuropathol Exp Neurol.* 1972;31:278–303.
3. Hatanaka H. Experience of boron-neutron capture therapy for malignant brain tumours—with special reference to the problems of postoperative CT follow-ups. *Acta Neurochir Suppl (Wien).* 1988;42:187–192.
4. Barth RF, Vicente MG, Harling OK, et al. Current status of boron neutron capture therapy of high grade gliomas and recurrent head and neck cancer. *Radiat Oncol.* 2012;7:146–166.
5. Barth RF. Boron neutron capture therapy at the crossroads: challenges and opportunities. *Appl Radiat Isot.* 2009;67(suppl):S3–S6.
6. Barth RF, Yang W, Huo T, et al. Comparison of intracerebral delivery of carboplatin and photon irradiation with an optimized regimen for boron neutron capture therapy of the F98 rat glioma. *Appl Radiat Isot.* 2011;69:1813–1816.
7. Barth RF, Coderre JA, Vicente MG, Blue TE. Boron neutron capture therapy of cancer: current status and future prospects. *Clin Cancer Res.* 2005;11:3987–4002.
8. Soloway AH, Tjarks W, Barnum BA, et al. The chemistry of neutron capture therapy. *Chem Rev.* 1998;98:1515–1562.
9. Black KL, Ningaraj NS. Modulation of brain tumor capillaries for enhanced drug delivery selectively to brain tumor. *Cancer Control.* 2004;11:165–173.
10. Sköld K, H-Stenstam B, Diaz AZ, Giusti V, Pellettieri L, Hopewell JW. Boron neutron capture therapy for glioblastoma multiforme: advantage of prolonged infusion of BPA-f. *Acta Neurol Scand.* 2010;122:58–62.
11. Miyatake S, Kawabata S, Yokoyama K, et al. Survival benefit of boron neutron capture therapy for recurrent malignant gliomas. *J Neurooncol.* 2009;91:199–206.
12. Miyatake S, Tamura Y, Kawabata S, Iida K, Kuroiwa T, Ono K. Boron neutron capture therapy for malignant tumors related to meningiomas. *Neurosurgery.* 2007;61:82–90.
13. Kawabata S, Hiramatsu R, Kuroiwa T, Ono K, Miyatake S. Boron neutron capture therapy for recurrent high-grade meningiomas. *J Neurosurg.* 2013;119:837–844.
14. Sköld K, Gorlia T, Pellettieri L, Giusti V, H-Stenstam B, Hopewell JW. Boron neutron capture therapy for newly diagnosed glioblastoma multiforme: an assessment of clinical potential. *Br J Radiol.* 2010;83:596–603.
15. Kankaanranta L, Seppala T, Koivunoro H, et al. L-Boronophenylalanine-mediated boron neutron capture therapy for malignant glioma progressing after external beam radiation therapy: a phase I study. *Int J Radiat Oncol Biol Phys.* 2011;80:369–376.
16. Barth RF, Yang W, Bartus RT, et al. Neutron capture therapy of intracerebral melanoma: enhanced survival and cure after blood-brain barrier opening to improve delivery of boronophenylalanine. *Int J Radiat Oncol Biol Phys.* 2002;52:858–868.
17. Barth RF, Yang W, Rotaru JH, et al. Boron neutron capture therapy of brain tumors: enhanced survival following intracarotid injection of either sodium borocaptate or boronophenylalanine with or without blood-brain barrier disruption. *Cancer Res.* 1997;57:1129–1136.
18. Hsieh CH, Chen YF, Chen FD, et al. Evaluation of pharmacokinetics of 4-borono-2-$^{18}$F-fluoro-l-phenylalanine for boron neutron capture therapy in a glioma-bearing rat model with hyperosmolar blood–brain barrier disruption. *J Nucl Med.* 2005;46:1858–1865.
19. Abbott NJ, Romero IA. Transporting therapeutics across the blood-brain barrier. *Mol Med Today.* 1996;2:106–113.
20. Kroll RA, Neuwelt EA. Outwitting the blood-brain barrier for therapeutic purposes: osmotic opening and other means. *Neurosurgery.* 1998;42:1083–1099.
21. Yang FY, Lee PY. Efficiency of drug delivery enhanced by acoustic pressure during blood-brain barrier disruption induced by focused ultrasound. *Int J Nanomedicine.* 2012;7:2573–2582.
22. Yang FY, Wang HE, Lin GL, Lin HH, Wong TT. Evaluation of the increase in permeability of the blood-brain barrier during tumor progression after pulsed focused ultrasound. *Int J Nanomedicine.* 2012;7:723–730.
23. Yang FY, Lin GL, Horng SC, et al. Pulsed high-intensity focused ultrasound enhances the relative permeability of the blood-tumor barrier in a glioma-bearing rat model. *IEEE Trans Ultrason Ferroelectr Freq Control.* 2011;58:964–970.
24. Yang FY, Liu SH, Ho FM, Chang CH. Effect of ultrasound contrast agent dose on the duration of focused-ultrasound-induced blood-brain barrier disruption. *J Acoust Soc Am.* 2009;126:3344–3349.
25. McDannold N, Vykhodtseva N, Hynynen K. Effects of acoustic parameters and ultrasound contrast agent dose on focused-ultrasound induced blood-brain barrier disruption. *Ultrasound Med Biol.* 2008;34:930–937.
26. Yang FY, Horng SC, Lin YS, Kao YH. Association between contrast-enhanced MR images and blood-brain barrier disruption following transcranial focused ultrasound. *J Magn Reson Imaging.* 2010;32:593–599.
27. Yang FY, Teng MC, Lu M, et al. Treating glioblastoma multiforme with selective high-dose liposomal doxorubicin chemotherapy induced by repeated focused ultrasound. *Int J Nanomedicine.* 2012;7:965–974.
28. Yang FY, Wong TT, Teng MC, et al. Focused ultrasound and interleukin-4 receptor-targeted liposomal doxorubicin for enhanced targeted drug delivery and antitumor effect in glioblastoma multiforme. *J Control Release.* 2012;160:652–658.
29. Yang FY, Chen YW, Chou FI, Yen SH, Lin YL, Wong TT. Boron neutron capture therapy for glioblastoma multiforme: enhanced drug delivery and antitumor effect following blood-brain barrier disruption induced by focused ultrasound. *Future Oncol.* 2012;8:1361–1369.

30. Yang FY, Wang HE, Lin GL, et al. Micro-SPECT/CT–based pharmacokinetic analysis of $^{99m}$Tc-diethylenetriaminepentaacetic acid in rats with blood–brain barrier disruption induced by focused ultrasound. *J Nucl Med.* 2011;52:478–484.
31. Yang FY, Wang HE, Liu RS, et al. Pharmacokinetic analysis of $^{111}$In-labeled liposomal doxorubicin in murine glioblastoma after blood-brain barrier disruption by focused ultrasound. *PLoS One.* 2012;7:e45468.
32. Wang HE, Liao AH, Deng WP, et al. Evaluation of 4-borono-2-$^{18}$F-fluoro-L-phenylalanine-fructose as a probe for boron neutron capture therapy in a glioma-bearing rat model. *J Nucl Med.* 2004;45:302–308.
33. Yang FY, Lin YS, Kang KH, Chao TK. Reversible blood-brain barrier disruption by repeated transcranial focused ultrasound allows enhanced extravasation. *J Control Release.* 2011;150:111–116.
34. Loening AM, Gambhir SS. AMIDE: a free software tool for multimodality medical image analysis. *Mol Imaging.* 2003;2:131–137.
35. Imahori Y, Ueda S, Ohmori Y, et al. Positron emission tomography-based boron neutron capture therapy using boronophenylalanine for high-grade gliomas: part II. *Clin Cancer Res.* 1998;4:1833–1841.
36. Yoshino K, Suzuki A, Mori Y, et al. Improvement of solubility of *p*-boronophenylalanine by complex formation with monosaccharides. *Strahlenther Onkol.* 1989;165:127–129.
37. Ishiwata K, Shiono M, Kubota K, et al. A unique in vivo assessment of 4-[10B] borono-L-phenylalanine in tumour tissues for boron neutron capture therapy of malignant melanomas using positron emission tomography and 4-borono-2-[$^{18}$F] fluoro-L-phenylalanine. *Melanoma Res.* 1992;2:171–179.
38. Yang W, Barth RF, Rotaru JH, et al. Enhanced survival of glioma bearing rats following boron neutron capture therapy with blood-brain barrier disruption and intracarotid injection of boronophenylalanine. *J Neurooncol.* 1997;33: 59–70.
39. Yang W, Barth RF, Rotaru JH, et al. Boron neutron capture therapy of brain tumors: enhanced survival following intracarotid injection of sodium borocaptate with or without blood-brain barrier disruption. *Int J Radiat Oncol Biol Phys.* 1997;37:663–672.
40. Smith DR, Chandra S, Barth RF, Yang W, Joel DD, Coderre JA. Quantitative imaging and microlocalization of boron-10 in brain tumors and infiltrating tumor cells by SIMS ion microscopy: relevance to neutron capture therapy. *Cancer Res.* 2001;61:8179–8187.
41. Frenkel V, Etherington A, Greene M, et al. Delivery of liposomal doxorubicin (Doxil) in a breast cancer tumor model: investigation of potential enhancement by pulsed-high intensity focused ultrasound exposure. *Acad Radiol.* 2006;13: 469–479.